

# Effect of anesthesia carrier gas on *in vivo* circulation times of ultrasound microbubble contrast agents in rats

Lee Mullin<sup>a</sup>, Ryan Gessner<sup>a</sup>, James Kwan<sup>b</sup>, Mehmet Kaya<sup>a</sup>, Mark A. Borden<sup>b</sup> and Paul A. Dayton<sup>a\*</sup>

**Purpose:** Microbubble contrast agents are currently implemented in a variety of both clinical and preclinical ultrasound imaging studies. The therapeutic and diagnostic capabilities of these contrast agents are limited by their short *in-vivo* lifetimes, and research to lengthen their circulation times is on going. In this manuscript, observations are presented from a controlled experiment performed to evaluate differences in circulation times for lipid shelled perfluorocarbon-filled contrast agents circulating within rodents as a function of inhaled anesthesia carrier gas.

**Methods:** The effects of two common anesthesia carrier gas selections - pure oxygen and medical air were observed within five rats. Contrast agent persistence within the kidney was measured and compared for oxygen and air anesthesia carrier gas for six bolus contrast injections in each animal. Simulations were performed to examine microbubble behavior with changes in external environment gases.

**Results:** A statistically significant extension of contrast circulation time was observed for animals breathing medical air compared to breathing pure oxygen. Simulations support experimental observations and indicate that enhanced contrast persistence may be explained by reduced ventilation/perfusion mismatch and classical diffusion, in which nitrogen plays a key role by contributing to the volume and diluting other gas species in the microbubble gas core.

**Conclusion:** Using medical air in place of oxygen as the carrier gas for isoflurane anesthesia can increase the circulation lifetime of ultrasound microbubble contrast agents. Copyright © 2011 John Wiley & Sons, Ltd.

**Keywords:** anesthesia; carrier gas; microbubble; lifetime; persistence; circulation time

## 1. Introduction

Microbubble contrast agents (MCAs) are currently implemented in many ultrasound imaging studies to provide enhanced resolution of a vascular network (1–3) as well as to act as vehicles for therapeutic applications (4,5). These contrast agents are lipid-encapsulated gaseous microspheres, ranging in diameter from 1 to 10  $\mu\text{m}$ . Their ability to improve an image's quality is due to the difference in acoustic impedance between their gaseous core and the surrounding medium. The impedance difference, as well as their compressibility, causes MCAs to be very echogenic, where even a single microbubble can be detected (5–7).

The nonlinear behavior of MCAs in response to ultrasound pulses allows their scattered echoes to be separable from tissue, providing a high contrast to tissue ratio. MCAs have been applied in a wide range of imaging studies including assessing myocardial perfusion (8,9), imaging blood-perfusion in tumors (10,11) and molecular targeting of angiogenesis or inflammation (12–15).

Other applications of microbubble vehicles include acting as therapeutic delivery mediators, where microbubbles carry a gene or drug on or within their shell (4,16–18). Microbubbles can also be applied in conjunction with therapeutic compounds to enhance drug or gene delivery across the vascular endothelium (6).

The ability of an MCA to either enhance imaging of blood perfusion or act as therapeutic mediator is maintained only as

long as it is freely circulating and intact in the bloodstream, or intentionally deposited at a localized site. Therefore, if administration is through a bolus injection, the time window for ultrasound imaging or therapeutics is integrally correlated to the *in vivo* circulation times of the microbubbles. It has been hypothesized that the short *in vivo* and *in vitro* lifetimes of MCAs are a rate-limiting step for advancing ultrasound contrast technology as quickly as other contrast imaging modalities, such as X-ray and MRI (19). Under normal physiological conditions, an injected microbubble's lifetime is a function of both compositional and environmental variables. Studies have shown that the makeup of a bubble's lipid shell and the content of the gas core affect its lifetime (20,21), while environmental factors such as the acoustic waveforms incident on the bubble (22), dissolved gas concentration in the blood (23,24), and immune response (25) also play critical roles. Recent attempts to improve the composition of microbubbles include using higher

\* Correspondence to: P. A. Dayton, UNC-NCSU Joint Department of Biomedical Engineering, 304 Taylor Hall, CB 7575, Chapel Hill, NC 27599, USA.  
E-mail: padayton@bme.unc.edu

<sup>a</sup> L. Mullin, R. Gessner, M. Kaya, P. A. Dayton  
Joint Department of Biomedical Engineering, University of North Carolina and North Carolina State University, Chapel Hill, NC 27599, USA

<sup>b</sup> J. Kwan, M. A. Borden  
Department of Chemical Engineering, Columbia University, New York, NY 10027, USA

molecular weight and less soluble filling gasses (21,26), and altering the chemical composition of the microbubble's lipid shell (27,20). Increasing the circulation lifetimes would improve the ability to perform consistent imaging studies over time with a bolus injection, as well as improve the window in which both diagnostic and therapeutic applications can be applied.

One possible method to improve the environmental conditions for injected MCAs during studies in anesthetized animals is by changing the dissolved gas concentration of an animal's blood. It is well known that the gas saturation in the medium surrounding the microbubble affects the gas core's dissolution rate (27–29). Early studies with first-generation contrast agents demonstrated that MCAs circulating in dogs that inhaled different anesthesia carrier gases had different circulation times (23,24). These previous studies examined two albumin-shelled agents, Albunex and Optison, and observed circulation persistence for different ratios of two common selections for anesthesia carrier gas: medical air and pure oxygen. In both studies, the imaging contrast provided by these two types of MCAs was diminished by the use of pure oxygen as a carrier gas compared with the contrast provided by the same MCA type in the same animal breathing medical air as the carrier gas.

In this paper we extend these early studies from albumin-shelled contrast agents to newer lipid-shelled perfluorocarbon-filled contrast agents. Additionally, we examine the effects of inhaled anesthesia gas on injected MCAs in a rodent model. Rodents are commonly used as preclinical models of cancer and other diseases, and as such, are frequently selected as subjects in ultrasound contrast imaging studies. The purpose of this study was to elucidate the extent and significance of the relationship between anesthesia carrier gas composition and MCA circulation lifetime in rats.

## 2. Results and discussion

### 2.1. The effect of carrier gas composition on MCA lifetime *in vivo*

Six imaging studies were completed for each animal, with each study consisting of a single bolus injection of contrast. Circulation times, obtained from intensity curves (Fig. 1), were compared for medical air and oxygen. A statistically significant difference ( $p < 0.05$ ) was observed for MCA circulation time as a function of anesthesia carrier gas in four out of five animals (Fig. 2). Circulation time in the cases for which the data was not significant illustrated the same trend as in the other animals. Administering medical air as the anesthesia carrier gas caused the contrast agent half-life to be an average of  $1.8 \pm 0.1$  times longer than when using pure oxygen. A greater difference was observed when examining time to 25% peak intensity; the  $t_{0.25\text{Imax}}$  was  $2.2 \pm 0.2$  times longer when the animal was breathing medical air compared with breathing pure oxygen.

### 2.2. Relationships between carrier gas and physiology

Dissolved blood oxygen and carbon dioxide gas partial pressures were measured in four animals to observe any partial pressure differences between animals breathing pure oxygen and medical air (Table 1). The largest effect of carrier gas on these variables was with  $p\text{O}_2$ , as the average value was over six times higher when breathing oxygen compared to medical air. The sum of partial pressures ( $\Sigma p_i$ ) indicated a greater degree of ventilation/

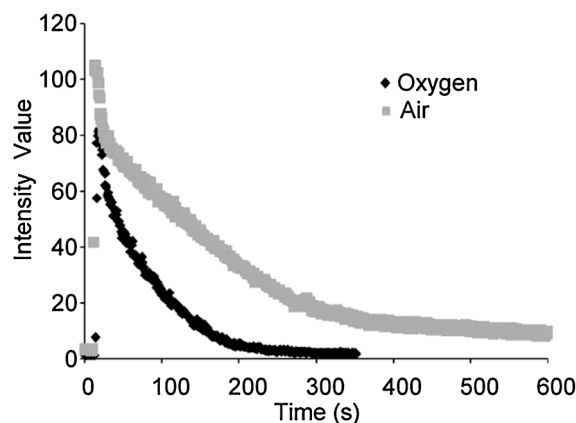


**Figure 1.** A comparison of intensity curves obtained from animal 3 while breathing air compared with breathing oxygen is shown. The differences between the intensity curves is representative of results seen in all animals.

perfusion mismatch for oxygen-breathing rats than for air-breathing rats, as may be expected (30,31).

One might hypothesize that the longer circulation times may be due to vasculature changes induced by the different inhaled anesthesia carrier gases. However, based on the measured blood gas values, shown in Table 1, it does not appear that vascular changes are contributing to the increased MCA circulation lifetime.  $\text{CO}_2$  partial pressure levels have been shown to be related to changes in vasculature dilation (32), but these values stayed relatively constant regardless of the administered carrier

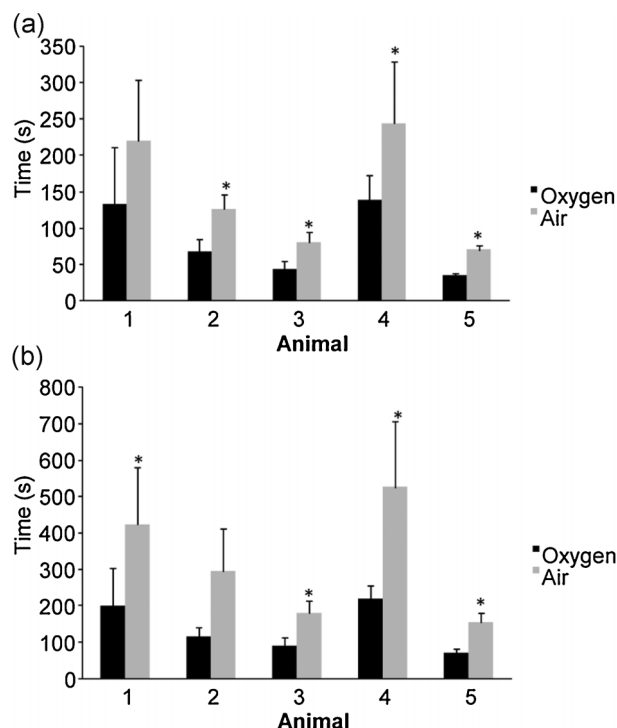


**Figure 2.** Side by side comparison of the average injected MCA circulation times for each animal. (A) Average half-life and (B) average time to 25% for each animal inhaling the respective anesthesia carrier gases. The average circulation times when an animal was breathing isoflurane carried by medical air were significantly longer in most animals (\* $p < 0.05$ ).

**Table 1.** Mean partial pressures of dissolved O<sub>2</sub> and CO<sub>2</sub> gasses in arterial blood were measured from animals anesthetized with the two different carrier gases

	pO <sub>2</sub> (mmHg)	pCO <sub>2</sub> (mmHg)	pN <sub>2</sub> (mmHg)	pH <sub>2</sub> O (mmHg)	Σp <sub>i</sub> (mmHg)
Normal range	80–100	32–45	555–585	47	714–777
Breathing air (n = 4)	70 ± 6	63 ± 9	560	47	740
Breathing oxygen (n = 3)	546 ± 45	61 ± 15	0	47	654

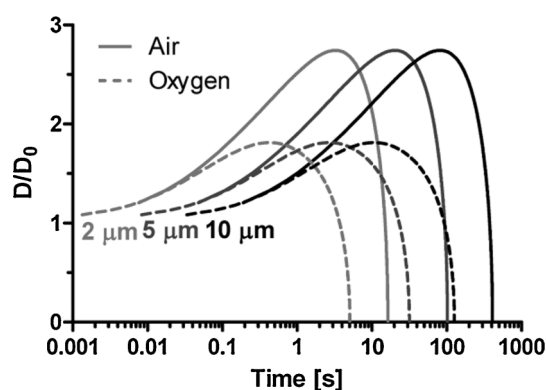
The values for N<sub>2</sub> and H<sub>2</sub>O were taken from literature (30,31). Σp<sub>i</sub> is the sum of partial pressures. The pO<sub>2</sub> increased above the normal range while breathing pure oxygen, but the pCO<sub>2</sub> remained constant. Ventilation/perfusion mismatch increased for rats breathing pure oxygen, as expected (30,31). These values were used to simulate the dissolution times of a single MCA within the different mixed gas environments.

gas. Other factors that could potentially influence circulation time, such as breathing rate, heart rate and body temperature, were investigated. Preliminary studies (data not shown) showed no correlation between breathing rate, heart rate, body temperature and circulation times.

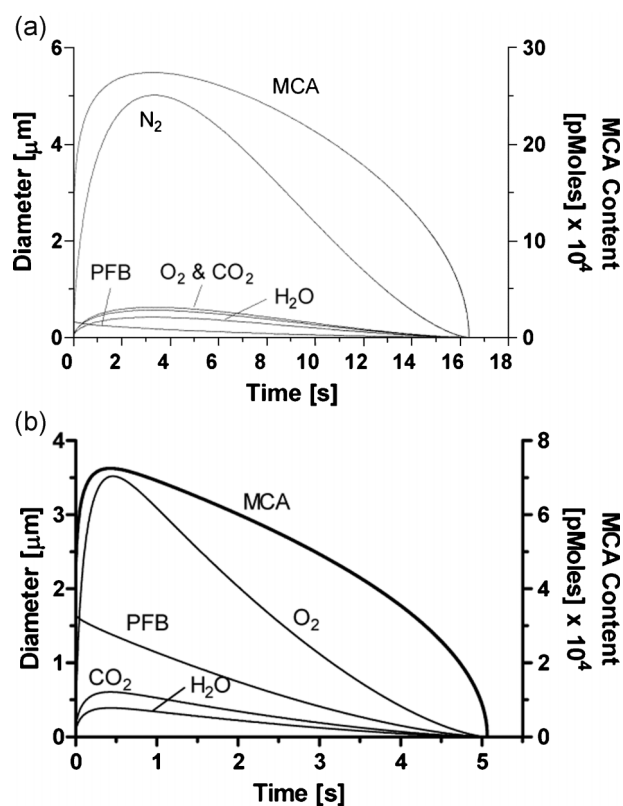
### 2.3. Simulations of MCA circulation time

To gain physical insight, we modeled microbubble dissolution times in blood by considering pure diffusion (no convection) of the different gas species into and out of the bubbles, as others have reported previously (33,34). Equations (1) and (2) were solved numerically using the Newton–Raphson method and MATLAB software (MathWorks, Natick, MA) for a 2, 5 and 10 μm diameter microbubble initially filled with pure perfluorobutane (PFB) and suddenly immersed in blood. Blood gas (O<sub>2</sub>, N<sub>2</sub>, H<sub>2</sub>O and CO<sub>2</sub>) partial pressure values were taken from Table 1 to simulate oxygen vs air as the carrier gas. The surface tension was set to 0 mN/m (28), and the hydrostatic pressure was set to 760 mmHg.

Figure 3 shows the simulation results for the two carrier gases. Theory predicted that a 2 μm diameter microbubble survives approximately 3.2 times longer when medical air is used instead of oxygen (Fig. 3). As the diameter was increased to 10 μm, the microbubble lifetimes were predicted to be 126 s for oxygen-breathing and 409 s for air-breathing, which was in good general agreement with the experimental *in vivo* imaging data. Inspection of the microbubble contents over time provided an

**Figure 3.** Simulated response of a PFB microbubble suddenly immersed in arterial blood. The dissolved gas parameters used in these simulations, summarized in Table 1, were based on measured values. Microbubble diameter was normalized by the initial value shown.

explanation for the extended lifetime (Fig. 4). Initially, the blood gases rapidly diffused into the microbubble just as PFB, which has a much lower solubility and diffusivity in water, slowly dissolved away. The influx of blood gases resulted in rapid microbubble growth. Microbubble growth could not be measured acoustically here due to the complexity of the *in vivo* backscattered signal. However, microbubble growth has been predicted and measured as an increase in ultrasound attenuation in a more idealized system by Sarkar *et al.* (35,36). The presence of nitrogen extended the growth phase by not only adding to the volume, but also diluting the other gas species, resulting in greater accumulation of the other blood gases and reduction in the rate of PFB efflux. After a short time, the microbubble was mainly composed of

**Figure 4.** Simulated response of a PFB microbubble suddenly immersed in arterial blood. The dissolved gas parameters used in these simulations, summarized in Table 1, were based on measured values. Molar contents of each gas are plotted vs time for (A) medical air and (B) oxygen as the carrier gas.

blood gases, and PFB contributed only slightly to the total volume. Eventually, all gases began to efflux from the microbubble as PFB dissolution continued and the partial pressures of O<sub>2</sub>, N<sub>2</sub> and CO<sub>2</sub> in the gas core exceeded the partial pressures in the surrounding blood. The dissolution rate was accelerated for the oxygen-carrier case owing to the greater degree of ventilation/perfusion imbalance. The sum of the partial pressures for oxygen-breathing (653 mmHg) was much lower than for air-breathing (740 mmHg). Since the ambient pressure was approximated to be 760 mmHg, the oxygen-breathing case represented a greater deviation from equilibrium and therefore a greater driving force for microbubble dissolution.

We should note that the simplified model is limited when making direct comparisons to *in vivo* contrast persistence data. The calculation ignores the gas permeation resistance of the shell and assumes a constant surface tension (although near zero), which may not be true during the multiple regions of growth and dissolution that bubbles would experience (37). Additionally, the calculations only take into account a single bubble under no-flow conditions. It is possible that a population of bubbles is more stable than a single bubble. The overlapping diffusion zones between neighboring microbubbles will influence their rate of dissolution, and there may be more subtle effects at play such as Ostwald ripening. These assumptions, along with activity of other clearance mechanisms like the reticuloendothelial system (RES), could account for observed circulation times being longer than the model predicts. Despite the limitations of the model, it clearly illustrates different responses due to different gases, which agrees with experimental data.

### 3. Conclusions

A relationship between the anesthesia carrier gas and the *in vivo* lifetime of injected MCAs was observed within the five animals tested in this study. Each animal was administered three doses of MCAs under each type of carrier gas – medical air and pure oxygen – and the persistence of these contrast agents was monitored following injection. Half-life values and time to 25% intensity were calculated. Medical air was found to significantly increase the circulation time of ultrasound MCAs. The numerical results obtained using a model obeying classical Fickian diffusion with multiple gas species aligned with the experimentally measured values, suggesting that diffusion plays a key role in the reduced circulation time of injected MCAs in pure oxygen-breathing animals. The effects of diffusion for the oxygen-breathing case are manifest as an increased driving force (i.e. ventilation/perfusion mismatch) and more rapid mass transfer (i.e. absence of an inert ‘filling’ gas) for microbubble dissolution. This study illustrated that a simple change of an anesthesia carrier gas has the potential to improve the efficacy of ultrasound studies, both imaging and therapeutic.

## 4. Experimental

### 4.1. Gas diffusion model

To investigate whether gas diffusion could account for differences in MCA lifetime, a mathematical model previously developed by Kwan and Borden (37) was employed which predicts the size of a microbubble suddenly immersed in a multi-gas environment, such as a PFB microbubble injected into

blood. This model assumes that each gas acts independently to equilibrate at the gas–liquid interface and diffuse along its own chemical potential (partial pressure) gradient. All gases contribute to the total pressure and volume of the MCA gas core. Gas diffusion occurs through a stagnant aqueous layer equal in thickness to the microbubble radius (i.e. it is a purely diffusing sphere). Because the animal was breathing, the impact of the microbubble injection (~2 µl gas) on the dissolved gas contents of the blood pool was considered negligible. A set of coupled, nonlinear differential equations results from (i) a species balance over the microbubble, (ii) the diffusion equation, (iii) the Laplace pressure equation and (iv) the ideal gas law. Applying a finite difference method, the set of equations is discretized to the following form:

$$n_i^{\tau+1} = -4\pi h R D_i K_{H,i} \left[ \frac{2\sigma}{R} - P_{\infty,i} f_i + P_H - \frac{3BT}{4\pi R^3} \sum_{j=1}^N n_j \right] + n_i, \quad j \neq i \quad (1)$$

$$0 = \frac{8\pi\sigma}{3BT} (R^{\tau+1})^2 + \frac{4\pi P_H}{3BT} (R^{\tau+1})^3 - \sum_{i=1}^N n_i^{\tau+1} \quad (2)$$

where  $N$  is the total number of gas species;  $\tau$  is the numerical time step;  $R$  is the microbubble radius;  $\sigma$  is the microbubble surface tension;  $P_H$  is the hydrostatic pressure;  $B$  is the universal gas constant;  $T$  is temperature;  $n_i$  is the moles;  $D_i$  is the diffusion coefficient;  $K_{H,i}$  is Henry's constant;  $P_{\infty,i}$  is the partial pressure at saturation; and  $f_i$  is the ratio of the bulk dissolved gas content to that at saturation, each of component  $i$ . Solving equations (1) and (2) numerically allows prediction of the growth and dissolution of a microbubble subject to the simultaneous influx and efflux of different gas species as the system tends toward thermodynamic equilibrium, which occurs when the partial pressures in the gas core and surrounding medium are equal for all species. A variable time step was used to ensure that the moles inside the microbubble did not become negative. To determine the number of moles in the bubble, a forward wind difference method was applied, as seen in equation (1), which is solved step-wise. Equation (2) is non linear and was solved using a Newton–Raphson method (100 iterations). In the simulation, 100 iterations were used in the Newton–Raphson method. Finally, it should be noted that the model is limited in that it neglects the effects of convection in the surrounding medium, variations in blood gas concentrations and pressure as the microbubble passes through the venous–arterial circuit, and effects of the encapsulating shell, such as gas permeation resistance and viscous and elastic terms accounting for lipid monolayer expansion, break-up, compression, buckling and collapse.

### 4.2. Animal preparation

Animals were handled according to National Institute of Health guidelines and our study protocol was approved by the UNC Institutional Animal Care and Use Committee. Five female Sprague–Dawley rats (Harlan; Indianapolis, IN, USA) were imaged throughout the course of this study. Before imaging an animal, it was first anesthetized in an induction chamber by introducing an aerosolized 5% isoflurane–oxygen mixture. Once sedated, the animal was removed from the induction chamber, the isoflurane concentration was reduced from 5 to 2% and then maintained via mask delivery. Its abdomen was shaved with an electric clipper and a depilating cream was applied to the animal's skin to dissolve any remaining hair that would interfere with the



ultrasound image. A 24 gauge catheter was then inserted into the animal's tail vein for the administration of MCAs. The animal was placed in dorsal recumbency on a heating pad, and ultrasound coupling gel was placed between the imaging transducer and the animal's skin to ensure the quality of signal transmission.

### 4.3. Contrast agent preparation and administration

A lipid mixture {1,2-distearoyl-sn-glycero-3-phosphocholine (DSPC); 1,2-distearoyl-sn-glycero-3-phosphoethanolamine-*N*-[methoxy-(polyethylene glycol)-2000] (ammonium salt; DSPE-PEG2000; Avanti Polar Lipids)} was prepared using a 9:1 molar ratio, similar to a previously described method (20). Briefly, lipids were dissolved in chloroform, dried and dissolved into a buffer solution of PBS. The lipid solution was then transferred into vials, which were then evacuated and filled with decafluorobutane gas. Vials were shaken with a Vialmix shaker (Bristol-Myers Squibb Medical Imaging, North Billerica, MA, USA) for 45 s prior to injection. MCAs, of mean diameter  $0.84 \pm 0.34 \mu\text{m}$ , were withdrawn directly from the vial with the vial vent connected to a bag filled with decafluorobutane, to ensure that no air entered the headspace of the vial. Aliquots of 25  $\mu\text{l}$  of MCAs were administered through the tail vein, followed immediately by a 200  $\mu\text{l}$  flush of sterilized saline.

### 4.4. Image acquisition

The kidneys of the rats were selected as the imaging location for this study because of their proximity to the skin's surface and the high concentration of vasculature. The clinical system used to acquire all ultrasound images in this study was an Acuson Sequoia 512 (Siemens, Mountain View, CA, USA). B-mode images were collected at 14 MHz using a linear array transducer (model 15L8). Contrast agents were imaged in CPS mode operating at 7 MHz and a mechanical index of 0.18. CPS provides a high contrast-to-tissue ratio while being minimally destructive to MCAs. Video data collection started prior to a bolus injection of MCAs, and continued for up to 20 min to allow a majority of the microbubbles to be cleared by the animal. If there were still MCAs visibly circulating in the image after 20 min, data collection was prolonged to accommodate the longer MCA persistence. Data by Killam *et al.* (38) showed that, after Optison injection into canines, the octafluoropropane was eliminated after a mean residence time of 38–46 s. As our model clearly shows, PFB rapidly dissolves from the microbubble and is replaced by the blood gases. It is therefore reasonable to assume that PFB is eliminated from the blood between contrast agent injections, which are 20 min apart. After the completion of all measurements for an animal, the imaging study was closed and the data exported from the ultrasound system in DICOM format. These files were later analyzed offline in MATLAB. Multiple imaging sequences were obtained of each anesthetized rat. An imaging sequence included the collection of two runs of data, one breathing oxygen and one breathing air, each beginning with an injection of MCAs and lasting until contrast agents were no longer visibly circulating. The order of carrier gas administration was randomized for all the animals. After the completion of the first run, the anesthesia carrier gas was changed and the animal was given 10 min to acclimate to this new carrier gas before initiating the second imaging sequence (24). The imaged sequence was repeated twice more to obtain a total of three imaging sequences for each carrier gas.

### 4.5. Monitoring physiological changes

Blood samples were collected to determine the extent of the relationship between dissolved blood gas partial pressures of oxygen, nitrogen, carbon dioxide and anesthesia carrier gas. Arterial blood samples were obtained from the tail and tested immediately after collection in a pH/blood gas analyzer (Chiron Diagnostics, Emeryville, CA, USA). Each sample was collected only after the animal had acclimated to the anesthesia carrier gas being tested.

### 4.6. Measuring microbubble circulation time

All video data were exported from the ultrasound system and imported into MATLAB for analysis. Regions of interest (ROIs) were defined around the perimeter of the kidney of each animal, and the mask applied to every frame of data. All data were examined to ensure there were no gross movements in tissue to cause inaccuracies in the ROI. The mean pixel intensity within the ROI was computed and plotted as a function of time. An example of this data is displayed in Fig. 1. To compute a pre-contrast baseline value, the mean pixel intensity of the ROI was averaged prior to the bolus injection of MCAs. After the MCAs were injected, the mean pixel intensity rose sharply to a single peak value as the bolus entered through the ROI, then decline as the bubbles became distributed throughout the animal's body and cleared from the system. As the population of injected MCAs began to decline, the grayscale pixel intensity in the ROI also decayed steadily from the initial peak down to the original baseline value. Using MATLAB, a fourth-order interpolation polynomial was fitted to the data following the peak value in the run.

Two metrics were used to quantify the circulation times of the injected MCAs: half-life and time to 25% intensity ( $t_{0.5\text{Imax}}$  and  $t_{0.25\text{Imax}}$  respectively). These were defined as the difference between the injection time (as determined by the highest mean intensity value in the dataset) and the times at which the data had dropped to the points either halfway to baseline ( $t_{0.5\text{Imax}}$ ) or 75% of the way to baseline ( $t_{0.25\text{Imax}}$ ) (25).

Measurements were repeated three times for each type of carrier gas on each animal to determine the effect of anesthesia carrier gas. These MCA circulation times for the two types of gases were compared between each animal. A paired two-sample Student's *t*-test was used to validate the statistical significance of the difference in circulation times of the injected MCAs between the two types of carrier gas.

## Acknowledgements

We would like to acknowledge Steven Feingold, Kennita Johnson and Zhikun Liu for animal handling and technical assistance provided during the collection of experimental data in this study. James Tsuruta prepared contrast agents used in this study. This study was supported in part from The NIH Roadmap for Medical Research, R21EB005325 to P.A.D., the NYSTAR James D. Watson Investigator Award to M.A.B., and R01EB009066 to both P.A.D. and M.A.B. Pilot studies for this research appear in the proceedings of the 2009 IEEE Ultrasonics Symposium, copyright IEEE.

## 5. Disclosure

P.A.D. is a member of the scientific advisory board for Targeson Inc.

## References

1. Cosgrove D. Ultrasound contrast agents: an overview. *Eur J Radiol* 2006; 60: 324–330.
2. Goldberg BB, Raichlen JS, Forsberg F. *Ultrasound Contrast Agents: Basic Principles and Clinical Applications*. Martin Dunitz: London, 2001.
3. Ohlerth S, O'Brien RT. Contrast ultrasound: general principles and veterinary clinical applications. *Vet J* 2007; 174: 501–512.
4. Ferrara K, Pollard R, Borden M. Ultrasound microbubble contrast agents: fundamentals and application to gene and drug delivery. *Annu Rev Biomed Eng* 2007; 9: 415–447.
5. Schneider M. Molecular imaging and ultrasound-assisted drug delivery. *J Endourol* 2008; 22: 795–802.
6. Sboros V. Response of contrast agents to ultrasound. *Adv Drug Deliv Rev* 2008; 60: 117–136.
7. Ophir J, Parker KL. Contrast agents in diagnostic ultrasound. *Ultrasound Med Biol* 1989; 15: 319–333.
8. Carr CL, Linder JR. Myocardial perfusion imaging with contrast echocardiography. *Echocardiography* 2008; 22: 795–802.
9. Schneider M. Design of an ultrasound contrast agent for myocardial perfusion. *Echocardiography* 2000; 17: S11–16.
10. Chomas JE, Pollard RE, Sadlowski AR, Griffey SM, Wisner ER, Ferrara KW. Contrast-enhanced US of microcirculation of superficially implanted tumors in rats. *Radiology* 2003; 229: 439–446.
11. Sugimoto K, Moriyasu F, Kamiyama N, Metoki R, Iijima H. Parametric imaging of contrast ultrasound for the evaluation of neovascularization in liver tumors. *Hepatol Res* 2007; 37: 464–472.
12. Dayton PA, Rychak JJ. Molecular ultrasound imaging using microbubble contrast agents. *Front Biosci* 2007; 12: 5124–5142.
13. Stieger SM, Dayton PA, Borden MA, Caskey CF, Griffey SM, Wisner ER, Ferrara KW. Imaging of angiogenesis using Cadence contrast pulse sequencing and targeted contrast agents. *Contrast Media Mol Imag* 2008; 3: 9–18.
14. Villanueva FS, et al. Myocardial ischemic memory imaging with molecular echocardiography. *Circulation* 2007; 115: 345–352.
15. Willmann JK, Lutz AM, Paulmurugan R, Patel MR, Chu P, Rosenberg J, Gambhir SS. Dual-targeted contrast agent for US assessment of tumor angiogenesis in vivo. *Radiology* 2008; 248: 936–944.
16. Hettiarachchi K, Zhang S, Feingold S, Lee AP, Dayton PA. Controllable microfluidic synthesis of multiphase drug-carrying lipospheres for site-targeted therapy. *Biotechnol Prog* 2009; 25(4): 938–945.
17. Postema M, Gilja OH. Ultrasound-directed drug delivery. *Curr Pharm Biotechnol* 2007; 8: 355–361.
18. Shortencarrier MJ, Dayton PA, Bloch SH, Schumann PA, Matsunaga TO, Ferrara KW. A method for radiation-force localized drug delivery using gas-filled lipospheres. *IEEE Trans Ultrason Ferroelectr Freq Control* 2004; 51: 822–831.
19. Soetanto K, Cham M. Study on the lifetime and attenuation properties of microbubbles coated with carboxylic acid salts. *Ultrasonics* 2000; 38: 969–977.
20. Borden MA, Kruse DE, Caskey CF, Zhao S, Dayton PA, Ferrara KW. Influence of lipid shell physicochemical properties on ultrasound-induced microbubble destruction. *IEEE Trans Ultrason Ferroelectr Freq Control* 2005; 52: 1992–2002.
21. Kabalnov A, et al. Dissolution of multicomponent microbubbles in the bloodstream: 2. Experiment. *Ultrasound Med Biol* 1998; 24(5): 751–760.
22. Chomas JE, Dayton P, Allen J, Morgan K, Ferrara KW. Mechanisms of contrast agent destruction. *IEEE Trans Ultrason Ferroelectr Freq Control* 2001; 48: 232–248.
23. Wible JH Jr, Wojdyla JK, Bales GL, McMullen WN, Geiser EA, Buss DD. Inhaled gases affect the ultrasound contrast produced by Albunex in anesthetized dogs. *J Am Soc Echocardiogr* 1996; 9: 442–451.
24. Wible J Jr, Wojdyla J, Bugaj J, Brandenburger G. Effects of inhaled gases on the ultrasound contrast produced by microspheres containing air or perfluoropropane in anesthetized dogs. *Invest Radiol* 1998; 33: 871–879.
25. Borden MA, Sarantos MR, Stieger SM, Simon SI, Ferrara KW, Dayton PA. Ultrasound radiation force modulates ligand availability on targeted contrast agents. *Mol Imag* 2006; 5: 139–147.
26. Riess J. Understanding the fundamentals of perfluorocarbons and perfluorocarbon emulsions relevant to in vivo oxygen delivery. *Artif Cells Blood Substit Immobil Biotechnol* 2005; 33: 47–63.
27. Borden MA, Longo ML. Dissolution behavior of lipid monolayer-coated, air-filled microbubbles: Effect of lipid hydrophobic chain length. *Langmuir* 2002; 18: 9225–9233.
28. Duncan PB, Needham D. Test of the Epstein–Plesset model for gas microparticle dissolution in aqueous media: effect of surface tension and gas undersaturation in solution. *Langmuir* 2004; 20: 2567–2578.
29. Talu E, Hettiarachchi K, Powell RL, Lee AP, Dayton PA, Longo ML. Maintaining monodispersity in a microbubble population formed by flow-focusing. *Langmuir* 2008; 24: 1745–1749.
30. Nunn JF. *Applied Respiratory Physiology*. Butterworths: London, 1987.
31. West JB. *Respiratory Physiology*. Williams and Wilkins: Philadelphia, PA, 1990.
32. Gambhir S, Inao S, Tadokoro M, Nishino M, Ito K, Ishigaki T, Kuchiaki H, Yoshida J. Comparison of vasodilatory effect of carbon dioxide inhalation and intravenous acetazolamide on brain vasculature using positron emission tomography. *Neurol Res* 1997; 19: 139–144.
33. Burkard ME, Van Liew HD. Oxygen-transport to tissue by persistent bubbles – theory and simulations. *J Appl Physiol* 1994; 77: 2874–2878.
34. Kabalnov A, Klein D, Pelura T, Schutt E, Weers J. Dissolution of multicomponent microbubbles in the bloodstream: 1. Theory. *Ultrasound Med Biol* 1998; 24: 739–749.
35. Chatterjee D, Jain P, Sarkar K. Ultrasound-mediated destruction of contrast microbubbles used for medical imaging and drug delivery. *Phys Fluids* 2005; 17: 100603–100608.
36. Sarkar K, Katiyar A, Jain P, Growth and. dissolution of an encapsulated contrast microbubble: effects of encapsulation permeability. *Ultrasound Med Biol* 2009; 35: 1385–1396.
37. Kwan JJ, Borden MA. Microbubble dissolution in a multigase environment. *Langmuir* 2010; 26: 6542–6548.
38. Killam AL, et al. Tissue distribution of I-125-labeled albumin in rats, and whole blood and exhaled elimination kinetics of octafluoropropane in anesthetized canines, following intravenous administration of OPTISON (R) (F5069). *Int J Toxicol* 1999; 18: 49–63.